Catalysis Science & Technology

Accepted Manuscript

ROYAL SOCIETY OF CHEMISTRY

www.rsc.org/catalysis

Journal Name

RSCPublishing

ARTICLE

Preparation of graphene supported highly-dispersed nickel nanoparticles for enhanced hydrogen generation from the ball-milled $LiBH_4$

Cite this: DOI: 10.1039/x0xx00000x

Received 00th September 2014,
Accepted 00th October 2014

DOI: 10.1039/x0xx00000x

www.rsc.org/

Juan Xu,[a,b,c] Yang Li,[a] Jianyu Cao,[*a] Rongrong Meng,[a] Wenchang Wang,[a] and Zhidong Chen[*a,b,c]

By a facile hydrogen thermal reduction method, highly-dispersed nickel nanoparticles (ca. 9.7 nm) were uniformly supported on graphene (Ni/G), and then ball-milled with $LiBH_4$ to intensively investigate their hydrogen storage behaviours. The Ni/G doped system exhibited a high gravimetric hydrogen capacity, excellent rehydrogenation reversibility and fast kinetics due to the synergetic effects of nanoconfinement in graphene and catalysis by Ni nanoparticles, demonstrating one promising strategy to design effective hydrogen storage materials from pristine $LiBH_4$. In the case of doping with 20 wt.% Ni/G, thermal dehydrogenation of $LiBH_4$ starts at ca. 180 ^oC and the main hydrogen release peaks are located at 275 and 465 ^oC, with a total weight loss of 15.2 wt.%. Furthermore, about 12.8 wt.% hydrogen can be desorbed in 45 min at 450 ^oC. More importantly, hydrogen released amount was kept at 12.6 wt.% in the second dehydrogenation process and a steady hydrogen capacity of ca. 9.8 wt.% in the 30th hydrogen uptake-release cycle was achieved under 3 MPa H_2 at 400 ^oC, proving that the Ni/G catalyst plays a crucial role in the improvement of the hydrogen uptake reversibility of $LiBH_4$ at lower temperature and pressure conditions. Especially, $LiBH_4$ was reformed and a new product, $Li_2B_{12}H_{12}$, was detected after the rehydrogenation process.

1 Introduction

Owing to its high energy density and clean combustion nature, hydrogen is considered as an ideal candidate for fossil fuel as energy carrier of the future, which can be effectively used in fuel cells to produce electricity. The largest challenge remaining in the development of sustainable hydrogen energy for on-board applications is to explore safe, efficient, renewable, light and affordable hydrogen storage solid materials that possess a high gravimetric capacity, long cyclical reversibility and fast kinetics.[1]

Because of the high theoretical gravimetric hydrogen capacity (18.5 wt.% H_2), lithium borohydride ($LiBH_4$) is widely considered as a promising hydrogen storage material for hydrogen-powered vehicles.[2] Unfortunately, pristine $LiBH_4$ is inadequate for mobile solid-state hydrogen storage applications due to its unfavourably high thermodynamic stability and too strong ionic bond strength. As reported in literature,[3] pristine $LiBH_4$ has a high onset temperature for hydrogen desorption (>400 ^oC), only a limited degree of hydrogen uptake even under 35 MPa hydrogen pressure at 600 ^oC, slow kinetics for both hydrogen release and uptake, and short cycle life. Therefore, many novel strategies such as the destabilization by catalysts doping, confinement in porous materials, or partial cation substitution have been extensively adopted to reduce the desorption enthalpy, enhance the dehydrogenation reaction kinetics and make the rehydrogenation reaction reversibility more achievable under reasonable conditions.[4]

Recently, many efficient catalysts, such as transition metals,[5-9] metal halides,[10-19] and metal oxides[20-22] have been comprehensively utilized to investigate their catalytic effects on the hydrogen storage properties of $LiBH_4$, which successfully brought about lowered onset temperature, increased dehydrogenation capacity, and improved rehydrogenation reversibility. Among these catalysts, nanometric Ni additives are considered as typical catalysts for $LiBH_4$ in virtue of their high catalytic effects, physical hydriding properties, low cost and good environmental friendliness.[5,23-26] For instance, the onset hydrogen release temperature can be decreased to ca. 300 ^oC and about 12.1 wt.% H_2 per $LiBH_4$ can be rehydrogenated in the first cycle at 600 ^oC under 10 MPa H_2 for 30 h by ball milling $LiBH_4$ and Ni with a molar ratio of 2:1.[23] However, many reported nickel catalysts were commercially obtained, so they are easy to be partially oxidized and agglomerated before use, as confirmed by various XRD patterns, XPS and morphology analysis. The addition of oxidized nickel nanoparticles would lead to a partial oxidation of $LiBH_4$, the appearance of irreversible products during the de-/rehydrogenation process and thus some deterioration of the hydrogen storage properties and cycle life.[26] Moreover, the particle size of these commercial nickel additives can reach to ~41 μm,[23] and their specific surface area is no more than 60.5

m^2 g^{-1},[25, 26] resulting into rather insufficient catalytic effect. Therefore, it is necessary to develop efficient and highly-dispersed nanometric Ni catalysts to destabilize $LiBH_4$.[5] As reported by Jongh et al, one very effective method to improve the catalytic effect of Ni in $LiBH_4$ is using high-surfaced carbon support to disperse nano-sized Ni.[27] By melt infiltrating 25 wt.% $LiBH_4$ into the nickel citrate solution pre-impregnated commercial porous graphitic carbon, about 9.2 wt.% hydrogen per $LiBH_4$ can be released at the second desorption process, but the catalyst content is large and the reaction process is not clear. From this point of view, using nanoporous carbon supported Ni as catalysts for destabilizing $LiBH_4$ is highly recommended because nano-sized Ni can effectively contact and react with $LiBH_4$ to simultaneously reduce the catalyst content, achieve high hydrogen release capacity, acquire reversible hydrogen uptake at moderate conditions and elucidate the most probable hydrogen release/uptake process.

Graphene, the first two-dimensional atomic crystal, emerges as a conceptually new class of carbon material, and its unique planar nanostructure and unusual properties (eg. high specific surface area and tunable pore structure) promise its potential applications in hydrogen energy storage.[28-30] Specifically, our work has demonstrated that graphene doped $LiBH_4$ showed better hydrogen release and uptake properties than commercial porous carbon doped $LiBH_4$.[31] Herein, highly-dispersed Ni nanoparticles were supported on graphene (Ni/G) by a facile H_2 thermal reduction method, and then ball-milled with $LiBH_4$ to systemically investigate their hydrogen storage behaviours, because as-prepared graphene possess huge surface area (~ 2340 m^2 g^{-1}) to uniformly disperse Ni NPs, and suitable pore size (mostly 3~5 nm) to confine $LiBH_4$ system.

2 Experimental methods

2.1 Materials

Commercial $LiBH_4$ (95% purity, J&K Chemical Ltd, Sweden), natural graphite (99.9995% purity, Alfa Aesar Ltd, UK), $Ni(NO_3)_2$·$6H_2O$ (99% purity, Sinopharm Chemical Reagent Co. Ltd, China), citric acid (99.5% purity, Acros), $NaNO_3$ (99% purity, Sinopharm Chemical Reagent Co. Ltd, China), $KMnO_4$ (99% purity, Sinopharm Chemical Reagent Co. Ltd, China), H_2SO_4 (96% purity, Sinopharm Chemical Reagent Co. Ltd, China), H_2O_2 (30% aqueous solution, Sinopharm Chemical Reagent Co. Ltd, China) and commercial Ni powders (99.5% purity, ca. 41 μm, Alfa Aesar Ltd, UK) were used as received.

2.2 Preparation of graphene using a microwave irradiation method

Graphene used in present study was prepared by a microwave irradiation[32] and thermo-reduction method. First of all, 1 g $NaNO_3$ and 1 g natural graphite powder were thoroughly mixed together and 35 mL H_2SO_4 was slowly added under violent stirring. Then, 5 g $KMnO_4$ was gradually added into the above mixture over about 1 h at room temperature so as to fully oxidize graphite powder to graphene oxide (GO). Subsequently, the GO sample was incorporated into a 100 mL 5 wt.% H_2SO_4 aqueous solution over about 2 h with gentle stirring, and then 100 mL 30 wt.% H_2O_2 was dropped. After being centrifuged and washed with a mixed aqueous solution of 3 wt.% H_2SO_4 and 0.5 wt.% H_2O_2, the GO powder obtained was irradiated for 1 min in a domestic microwave oven (1100 W) and then was filtrated, washed with deionized water and dried at 65 ^oC for 24 h. Afterwards, the above chemical activated GO powders were put in a tube furnace under flowing argon and heated at 800 ^oC for 1 h. Finally, the final products were then centrifuged, washed, and vacuum-dried.

2.3 Synthesis of Ni/G catalysts

First, 148.6 mg $Ni(NO_3)_2$·$6H_2O$ and 65.3 mg citric acid were jointly dissolved in 28 mL deionized water with gentle stirring. Then, 25 mg graphene was impregnated with 7.7 mL of the above solution for 3 h under static vacuum. After being vacuum dried at 120 ^oC for 12 h, the impregnated sample was thermally reduced by being dwelled at 400 ^oC for 1 h under a gas mixture of 10 vol.% H_2 in N_2. Finally, the Ni/G catalyst with a 25 wt.% Ni loading was obtained after filtration, washing and drying under vacuum at 70 ^oC for 8 h.

2.4 Doping $LiBH_4$ with Ni/G catalysts

$LiBH_4$ was doped with Ni/G catalysts by a facile ball milling method. Specifically, 20 wt.% Ni/G was mixed with $LiBH_4$ and 1 g mixtures were loaded into an agate milling vial and mechanically milled for 1.5 h using a Planetary QM-1SP2 ball miller under argon atmosphere at room temperature. The ball-to-power weight ratio was 30:1 at 580 rpm using stainless steel balls with 10 mm diameter. According to the same preparation process, pure graphene or commercial Ni NPs doped $LiBH_4$ was obtained. All the sample preparation was performed in an argon-filled glove box to keep H_2O and O_2 contamination below 1 ppm.

2.5 Structure and morphology characterization

The morphology of the Ni/G catalyst with a 25 wt.% Ni loading was analyzed by transmission electron microscopy (TEM) using a Technai G2 20s-Twin Microscope (FEP Inc., USA). Samples were prepared by dispersing the dry Ni/G powder in ethanol to form a homogeneous suspension, and then dropped on a 300-mesh copper grid for observation.

^{11}B nuclear magnetic resonance (NMR) and X-ray diffraction (XRD) measurements were carried out to investigate the structure change and infer the possible reaction process during the hydrogen uptake and release process. Diffraction patterns were collected on a Rigaku D/MAX-2500 diffractometer with Cu Kα radiation at a scanning rate of 2^o min^{-1} and with a step of 0.02^o. ^{11}B NMR data were collected using a Bruker Avance300 spectrometer.

Surface area and porosity of the graphene sample was obtained from N_2 adsorption-desorption isotherm and Barret-Joyner-Halenda (BJH) plots (Micromeritics porosimeter ASAP 2010).

2.6 Hydrogen releasing property measurements

In order to compare with the neat $LiBH_4$ system, the hydrogen capacity of the Ni/G doped $LiBH_4$ sample is calculated based only on the mass of pure $LiBH_4$, and the content of impurities and added Ni/G catalysts were not considered to the total weight.

Hydrogen desorption performance was investigated using a Netzsch STA449C TG-DSC thermoanalyzer coupled with a Balzers Thermostar Quadrupole Mass Spectrometer. Samples were heated at a rate of 10 °C min^{-1} under argon flowing with a purging rate of 20 cm^3 min^{-1}.

Cyclic hydrogen releasing properties were examined by volumetric method using a carefully calibrated Sievert's type apparatus. Typically, the 20 wt.% Ni/G doped LBH_4 sample was repeatedly dehydrogenated at 550 ^oC for 5 h, and

rehydrogenated at 400 °C with an initial 3 MPa hydrogen pressure for 10 h. As it is difficult to accurately characterize the rehydrogenation process under high hydrogen pressure, the restored hydrogen amounts were precisely determined in the subsequent dehydrogenation half-cycle.

3 Results and discussion

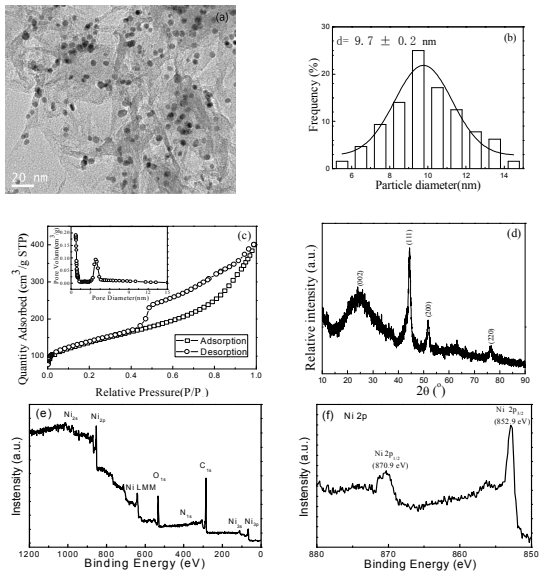

Fig. 1 TEM image (a), corresponding particle size distribution histogram (b), N_2 adsorption-desorption isotherm curve (c), pore size distribution plot (the inset), XRD pattern (d), XPS wide scan (e) and Ni 2p (f) spectra of as-prepared Ni/G.

The structure of Ni/G was characterized by transmission electron microscopy (TEM), N_2 adsorption-desorption, X-ray powder diffraction (XRD), X-ray photoelectron spectroscopy (XPS) and raman spectra. Fig. 1a and b show the micro-morphology and corresponding particle size distribution histogram of the Ni/G. As presented, well-dispersed Ni NPs are evenly distributed on large, disordered and over-lapped multilayer graphene sheets by a facile and cost-effective procedure. After randomly measuring more than 200 Ni NPs, it was found that the mean size of Ni NPs was ca. 9.7 nm and a relatively narrow particle size distribution was observed. No agglomerated Ni NPs were detected, proving that graphene with high specific surface area can effectively stabilize Ni NPs and prevent them from aggregation, which extremely contributes to the improvement in catalytic effect.[33-35] Fig. 1c displays the N_2 adsorption-desorption isotherm and corresponding pore-size distribution plot of the Ni/G, which was performed by coupling high-resolution nitrogen at 77.4 K. The Brunauer – Emmett - Teller (BET) specific surface area of the obtained Ni/G is about 242 $m^2 g^{-1}$, much higher than that of the commercial Ni NPs (ca. 60.5 $m^2 g^{-1}$).[25, 26] Moreover, the as-prepared Ni/G catalysts are porous materials[32] and the pore size distribution plot reveals that the pores in the Ni/G have a narrow micro-mesopores size distribution centred at ca. 3.8 nm (see the inset in Fig. 1c). The XRD pattern of Ni/G in Fig. 1d exhibits four diffraction peaks, which can be indexed to the diffraction from the (002) plane of graphene,[32] the (111), (200) and (220) planes of Ni NPs, respectively. Based on the half peak width of (111) plane and Scherrer equation, the crystallite size of Ni NPs was estimated to be ca. 9.8 nm, in good agreement with the TEM result. Furthermore, no NiO diffraction peak was observed in the XRD patterns. Fig. 1e and f illustrate XPS spectra of the Ni/G. The two peaks at about 285 eV and 535 eV are attributable to C 1s and O 1s in the Ni/G, respectively (Fig. 1e). In addition, the characteristic peaks of nickel element are observed and two peaks at 852.9 eV and 870.9 eV in the Ni 2p spectrum (Fig. 1f) are assigned to Ni $2p_{3/2}$ and Ni $2p_{1/2}$, respectively, which clearly indicate the presence of nickel after reduction.

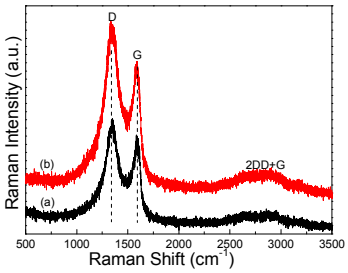

Fig. 2 Raman spectrum of graphene (a) and Ni/G (b).

Fig. 2 illustrates the Raman spectrum of graphene and Ni/G. Similar to chemically reduced graphenes and graphite nanoparticles, both graphene and Ni/G have two characteristic peaks at 1370 and 1570 cm^{-1}, which are assigned to the D band and G band, [36] respectively. Moreover, the raman spectrum of the Ni/G shows two weak peaks at ca. 2650 and 2910 cm^{-1}, which corresponds to the 2D and D+G bands. Based on the integration area of the D and G band peaks, the intensity ratio (ID/IG) of the Ni/G is 1.51, which is higher than that of graphenes (1.32), indicating a decrease in the size and a higher degree of disorder or defects. [37, 38] As reported in literature, [37] the increase in I_D/I_G may be attributed to the presence of Ni particles that can deter the recovery of sp^2 carbon domain and decrease the G band intensity of graphene.

Fig. 3 illustrates dehydrogenation performances of $LiBH_4$ that was respectively doped with graphene, commercial Ni NPs and Ni/G catalysts at a 20 wt.% doping amount, which was utilized to clarify the possible roles of graphene and Ni NPs in the catalytic dehydrogenation of $LiBH_4$. As observed, the first dehydrogenation temperature for the pure $LiBH_4$ sample starts at ca. 420 °C, while the two main desorption peaks are located at 485 and 610 °C with a weight loss of 10.7 wt.% (curve a). For the $LiBH_4$ doped with graphene, the initial temperature for main hydrogen desorption is ca. 230 °C, the temperatures for two major desorption peaks are 310 and 515 °C, and the weight loss corresponds to 11.4 wt.% (curve b), suggesting lower initial hydrogen desorption temperature than the pure $LiBH_4$, but the dehydrogenation capacity difference is small. In the case of the $LiBH_4$ doped with commercial Ni NPs, the first dehydrogenation temperature locates at ca. 310 °C, two main hydrogen desorption peaks occur at 420 and 605 °C, and 12.7 wt.% hydrogen can be released (curve c). By adding the Ni/G catalyst to $LiBH_4$, the initial dehydrogenation temperature of $LiBH_4$ transfers to 180 °C, and the main dehydrogenation peaks of $LiBH_4$ shift to 275 and 465 °C, with a greatly increased hydrogen released amount of 15.2 wt.% (curve d). As reported in literature,[27] the hydrogen release started at 200 °C, the maximum desorption peak located at 350 °C, and ca. 14 wt.% hydrogen was released for the Ni/porous carbon confined $LiBH_4$ using a melt infiltrating process. It is clear that the addition of Ni/G using a ball-milling process can better lower the hydrogen release temperature and improve hydrogen desorption amount.

Compared with the pristine $LiBH_4$, ball milling $LiBH_4$ with the graphene or Ni NPs decreased the main dehydrogenation temperature and enhanced the hydrogen release amount, proving a good destabilization effect on $LiBH_4$. Moreover, more hydrogen can be released from the commercial Ni NPs doped sample, and the graphene plays a more important role in reducing the onset dehydrogenation temperature of $LiBH_4$. More importantly, the Ni/G doped $LiBH_4$ possesses distinctly higher catalytic effect on $LiBH_4$ than graphene and Ni NPs alone, demonstrating that the obvious enhancement in hydrogen release properties should be attributed to the combined effect of graphene and Ni NPs. As confirmed in literatures,[27, 31] increased contact areas between the Ni/G catalysts and $LiBH_4$, newly produced structure defects during the ball-milling process and nanoconfinement effect in porous graphene materials help to remarkably improve the dehydrogenation properties of $LiBH_4$.

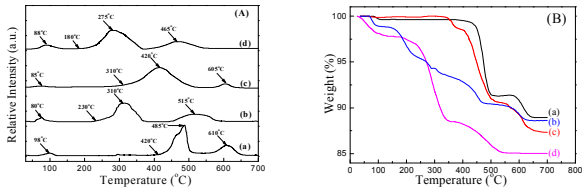

Fig. 3 Temperature programmed hydrogen release profiles (A) and TG curves (B) for pure $LiBH_4$ (a), graphene (b), commercial Ni NPs (ca. 41 μm) (c) and as-prepared Ni/G (d) doped $LiBH_4$ that were mechanically ball-milled under Ar atmosphere for 1.5 h. The doping amount of various catalysts is 20 wt.% and applied heating rate is 10 $^oC\ min^{-1}$.

Fig. 4 shows the first desorption curves of pristine $LiBH_4$ and various catalysts doped $LiBH_4$ at 450 °C. Within 90 min, only ca. 4.3 wt.% hydrogen was released from the pristine $LiBH_4$. In contrast, the graphene doped $LiBH_4$ sample gave out ca. 9.2 wt.% hydrogen and the addition of commercial Ni NPs into $LiBH_4$ resulted into ca. 10.4 wt.% hydrogen. For the Ni/G doped $LiBH_4$ sample, ca. 12.8 wt.% hydrogen can be desorbed and the hydrogen release amount can reach saturation in 45 min, indicating the Ni/G catalyst can substantially increase the H_2 release capacity from the mixture and reduce the desorption balance time. Evidently, both graphene and Ni NPs possess promoting effects on the dehydrogenation amount and kinetics of $LiBH_4$, and their synergistic effects can bring about better dehydrogenation performances.

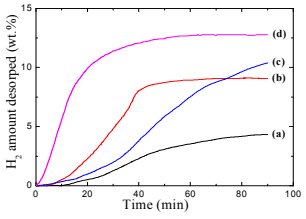

Fig. 4 Desorption curves under 0.1 MPa H_2 pressure at 450 °C for pristine $LiBH_4$ (a), graphene (b), commercial Ni NPs (ca. 41 μm) (c) and as-prepared Ni/G (d) doped $LiBH_4$. The doping amount of various catalysts is 20 wt.%.

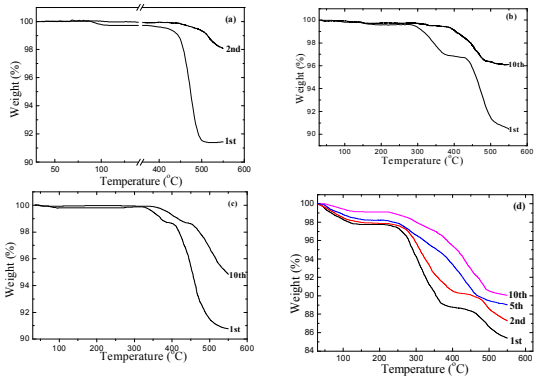

Fig. 5 Comparison on the dehydrogenation cycle profiles of pristine LBH_4 (a), graphene (b), commercial Ni NPs (ca. 41 μm) (c) and as-prepared Ni/G (d) doped $LiBH_4$. The doping amount of various catalysts is 20 wt.%. These doped $LiBH_4$ sample can be dehydrogenated (at 550 °C for 5 h) and rehydrogenated (at 3 MPa H_2, 400 °C for 10 h) repeatedly and measured gravimetrically.

In order to develop a reversible H_2 storage and release system for practical applications, the $LiBH_4$ samples doped with various catalysts were rehydrogenated at 400 °C for 10 h under 3 MPa H_2 after the dehydrogenation process at 550 °C for 5 h, and their cycling dehydrogenation properties were compared in detail, as shown in Fig. 5. Clearly, only 2.1 wt.% hydrogen could be restored after the first rehydrogenation for the pristine $LiBH_4$ sample (Fig. 5a). After doping with 20 wt.% graphene or commercial Ni NPs, about 4.0 wt.% and 5.2 wt.% hydrogen could be retrieved in the tenth cycle ((Fig. 5b and c), respectively. In contrast, for the 20 wt.% Ni/G doped $LiBH_4$, the total released H_2 amount gradually decreases from the initial 14.6 wt.% to the 12.6 wt.% in the second cycle, and further to 11.1 wt.% in the fifth cycle and to 9.8 wt.% in the tenth cycle ((Fig. 5d)). These results indicate that both graphene and Ni NPs can improve the reversibility of the $LiBH_4$ sample. Furthermore, the Ni/G doped $LiBH_4$ sample has the highest cyclic capacity and retention, which is attributable to the synthetic catalytic effect of graphene and Ni NPs.

Fig. 6 shows the cycle life of 20 wt.% graphene, commercial Ni NPs and Ni/G doped $LiBH_4$ sample. The H_2 capacity of the graphene and commercial Ni NPs doped $LiBH_4$ sample is 2.6 wt.% and 6.3 wt.% at the 30th dehydrogenation, demonstrating that the commercial Ni NPs have better catalytic effect on the capacity retention of $LiBH_4$. In the case of the Ni/G doped $LiBH_4$ sample, the reversible capacity is still kept at ca. 9.8 wt% after 30 hydrogen release and uptake cycles, which reaches the 2015 hydrogen storage target set by the DOE system: 9 wt. % H_2. These results demonstrate that the hydrogen release and uptake reversibility of $LiBH_4$ can be greatly improved by introducing both nanometric Ni catalysts and porous graphene materials.

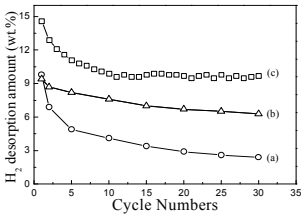

Fig. 6 Comparison on the cycle life of 20 wt.% graphene (a), commercial Ni NPs (b) and as-prepared Ni/G (c) doped $LiBH_4$.

To explore the catalytic effect of graphene and Ni NPs, we listed the initial and main hydrogen release temperature, and the first and 30th released hydrogen amount in Table 1. It was distinctly shown that ball-milling graphene with $LiBH_4$ lowers the hydrogen release temperature by 175 ^oC compared to the undoped $LiBH_4$, while the onset hydrogen release temperature was only decreased by 65 ^oC for the commercial Ni NPs doped $LiBH_4$. In the meantime, the main hydrogen release temperature of the graphene doped $LiBH_4$ is still obviously lower than the commercial Ni NPs doped $LiBH_4$. Thus, graphene has better catalytic effect on the decrease in hydrogen release temperature. On the other hand, it can be obviously concluded that Ni NPs helps to substantially enhance the hydrogen desorption amount based on the first and 30th released hydrogen amount. In the case of the Ni/G catalyzed sample, the initial hydrogen release temperature is lowered by 240 ^oC and reversible hydrogen amount can reach 9.8 wt. % in comparison with the undoped $LiBH_4$, which come from the synergic effect of graphene and Ni NPs.

Table 1 - Hydrogen release properties of the different catalysts doped LiBH4 with the same mass ratios.

Sample	Onset Tdesorb (^oC)	Main Tdesorb (^oC)	H_2 desorbed (wt. %)	30th H_2 desorbed (wt. %)
$LiBH_4$	420	485; 610	10.7	< 1
graphene doped $LiBH_4$	230	310; 515	11.4	2.6
Ni NPs doped $LiBH_4$	310	420; 605	12.7	6.3
Ni/G doped $LiBH_4$	180	275;465	15.2	9.8

* Tdesorb represents the desorption temperature.

To figure out the enhancement in dehydrogenation capacity and kinetics, probe probable reaction process, and deduce possible structural change, ^{11}B NMR data and XRD patterns of the Ni/G doped $LiBH_4$ in the as-milled status, initial dehydrogenation condition at 550 °C for 5 h, and tenth rehydrogenation state at 400 °C for 10 h were acquired, as shown in Fig. 7. As shown in curve a of Fig. 7A, a well-defined sharp peak at ca. -42 ppm was obtained from the as-milled sample, which can be denoted as one characteristic peak of $LiBH_4$.[39,40] After the dehydrogenation, several broaden peaks appear, suggesting that boron exists in an amorphous phase. Furthermore, the peak at ca. -42 ppm re-emerges in the rehydrogenation state, indicating that new $LiBH_4$ can be reformed.

After the ball-milling process, Ni, $LiBH_4$, LiH, LiC and broad C diffraction peaks were observed for the Ni/G doped $LiBH_4$ before the first dehydrogenation (curve a), indicating that the Ni/G catalyst can react with $LiBH_4$ to form LiC, and the minor appearance of LiH peaks may result from slight decomposition of $LiBH_4$ during the ball milling process. After the first dehydrogenation at 550 °C for 5 h, the $LiBH_4$ phase disappears, new phase Ni_4B_3 was detected and strong LiC, LiH and Ni diffraction peaks were identified (curve b). The possible hydrogen release reaction process for the Ni/G catalyzed sample may be expressed as $2LiBH_4 \rightarrow 2LiH + 2B + 3H_2$ and $3LiBH_4 + 3C + 4Ni \rightarrow 3LiC + Ni_4B_3 + 6H_2$. As for the rehydrogenated sample, $LiBH_4$ is reformed and one new product, $Li_2B_{12}H_{12}$,[5, 41] is detected (curve 3), confirming the reversible de-/rehydrogenation reactions. However, LiC and Ni_4B_3 phases still remain in the rehydrogenation state, indicating an incomplete rehydrogenation reaction, which may be the reason for the cyclic hydrogen capacity degradation of the Ni/G doped $LiBH_4$ sample from the initial 15.2 wt.% to 9.8 wt.% in the 30th dehydrogenation process. Based on the above XRD pattern of the rehydrogenated sample, it was inferred that the reversible hydrogen uptake course of the Ni/G doped $LiBH_4$ sample may be represented as follows: $2LiH+2B+3H_2 \rightleftharpoons 2LiBH_4$ and $12B+2LiH+ 5H_2 \rightleftharpoons Li_2B_{12}H_{12}$. By the way, no B peak is found in the dehydrogenated sample, which may due to its amorphous structure.[40] On the other hand, the crystallite size of Ni NPs was figured out to be ca. 9.6 nm after the ball-milling process, which was somewhat lower than the 9.8 nm of as-prepared Ni/G, while the value was increased to 14.7 and 16.8 nm for the first dehydrogenation and tenth dehydrogenated sample, respectively. The increase in the Ni diameter may derive from the hydrogen release and uptake process at 550 and 400 °C.

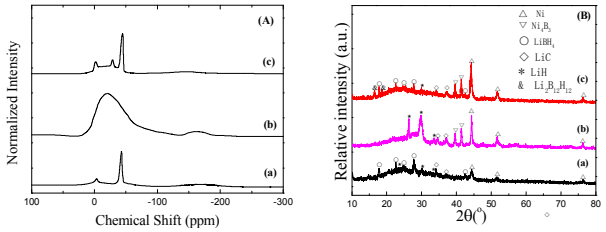

Fig. 7 ^{11}B NMR spectra (A) and XRD patterns (B) of the 20 wt.% Ni/G doped $LiBH_4$ in the as-milled condition(a), initial dehydrogenation status at 550 °C for 5 h(b), and tenth rehydrogenation state at 400 °C for 10 h(c).

4 Conclusions

The dehydrogenation-rehydrogenation cyclic performances and thermodynamics were dramatically enhanced upon mechanically ball milling $LiBH_4$ with Ni/G due to the combined effect of graphene and Ni NPs. Furthermore, it should be noted that the uniformly dispersed Ni NPs play a crucial role in improving the hydrogen desorption and uptake reversibility of $LiBH_4$ at reduced temperature and pressure conditions. Importantly, $LiBH_4$ is reformed and $Li_2B_{12}H_{12}$ is detected after being rehydrogenated at 400 °C under 3 MPa hydrogen pressure, with a capacity of approximately 9.8 wt.% in the 30th cycle. Thus, destabilizing $LiBH_4$ using the Ni/G catalyst is a new and promising way for the catalytic dehydrogenation and rehydrogenation of $LiBH_4$.

Acknowledgements

The authors gratefully acknowledge financial support from the National Science Foundation of China (21003015 and 21103014), the Science Foundation of Jiangsu Province (BK2012591 and 12KJA150003), the Foundation of Jiangsu Key Laboratory for Solar Cell Materials and Technology (201201), Graduate Students Cultivation, and Innovation project of Jiangsu Province (CXZZ12-0734), Qing Lan project of Jiangsu Province, the Priority Academic Program

Development of Jiangsu Higher Education Institutions (PAPD) and Jiangsu Key Laboratory of Advanced Catalytic Materials and Technology (BM2012110) for support of this work.

Notes and references

[a] Jiangsu Key laboratory of Advanced catalytic Materials and Technology, Jiangsu Key Laboratory of Materials Surface Science and Technology, Changzhou University, 1 Gehu Road, Changzhou 213164, PR China.
[b] Key Laboratory for Solar Cell Materials and Technology of Jiangsu Province, Changzhou University, 1 Gehu Road, Changzhou 213164, PR China.
[c] Qualtec Co. Ltd., Changzhou 213164, PR China.
Fax: 86-0519-86330239; Tel: 86-0519-86330239;
E-mail: jyucao@hotmail.com (J. Cao), cjytion3@163.com (Z. Chen)

1. C. Liang, Y. Liu, H. Fu, Y. Ding, M. Gao and H. Pan, *J. Alloys Compd.*, 2011, **509**, 7844–7853.
2. I. Saldan, *Cent. Eur. J. Chem.*, 2011, **9**, 761–775.
3. Y. Yan, A. Remhof, S. J. Hwang, H. W. Li, P. Mauron, S. Orimo and A. Züttel, *Phys. Chem. Chem. Phys.*, 2012, **14**, 6514–6519.
4. C. Li, P. Peng, D. W. Zhou and L. Wan, *Int. J. Hydrogen Energy*, 2011, **36**, 14512–14526.
5. P. Ngene, M. H. W. Verkuijlen, Q. Zheng, J. Kragten, P. J. M. van Bentum, J. H. Bitter and P. E. de. Jongh, *Faraday Discuss.*, 2011, **151**, 47–58.
6. J. Chen, Y. Zhang, Z. T. Xiong, G. T. Wu, H. L. Chu, T. He and P. Chen, *Int. J. Hydrogen Energy*, 2012, **37**, 12425–12431.
7. J. Mao, Z. Guo, X. Yu and H. Liu, *J. Alloys Compd.*, 2011, **509**, 5012–5016.
8. S. S. Deng, X. Z. Xiao, L. Y. Han, Y. Li, S. Q. Li, H. W. Ge, Q. D. Wang and L. X. Chen, *Int. J. Hydrogen Energy*, 2012, **37**, 6733–6740.
9. M. R. Ghaani, M. Catti and A. Nale, *J. Phys. Chem. C*, 2012, **116**, 26694−26699.
10. Y. F. Liu, H. Zhou, Y. F. Ding, M. X. Gao and H. G. Pan, *Funct. Mater. Lett.*, 2011, **4**, 395–399.
11. Y. Zhou, Y. Liu, W. Wu, Y. Zhang, M. Gao and H. Pan, *J. Phys. Chem. C*, 2012, **116**, 1588–1595.
12. Y. Zhou, Y. Liu, Y. Zhang, M. Gao and H. Pan, *Dalton Trans.*, 2012, **41**, 10980–10987.
13. J. H. Shim, Y. S. Lee, J. Y. Suh, W. Cho, S. S. Han and Y. W. Cho, *J. Alloys Compd.*, 2012, **510**, 9–12.
14. D. Blanchard, M. Zatti and T. Vegge, *J. Alloys Compd.*, 2013, **547**, 76–80.
15. R. Liu, D. Reed and D. Book, *J. Alloys Compd.*, 2012, **515**, 32–38.
16. J. Shao, X. Z. Xiao, L. X. Chen, X. L. Fan, S. Q. Li, H. W. Ge and Q. D. Wang, *J. Mater. Chem.*, 2012, **22**, 20764–20772.
17. D. Liu, J. Yang, J. Ni and A. Drews, *J. Alloys Compd.*, 2012, **514**, 103–108.
18. K. Jiang, X. Z. Xiao, L. X. Chen, L. Y. Han, S. Q. Li, H. W. Ge and Q. D. Wang, *J. Alloys Compd.*, 2012, **539**, 103–107.
19. S. T. Sabitu and A. J. Goudy, *Int. J. Hydrogen Energy*, 2012, **37**, 12301–12306.
20. A. Züttel, S. Rentsch, P. Fischer, P. Wenger, P. Sudan, P. Mauron and C. Emmenegger, *J. Alloys Compd.*, 2003, **356**, 515–520.
21. H. P. Yuan, X. G. Zhang, Z. N. Li, J. H. Ye, X. M. Guo, S. M. Wang, X. P. Liu and L. J. Jiang, *Int. J. Hydrogen Energy*, 2011, **37**, 3292–3297.
22. X. Chen, W. Cai, Y. Guo and X. Yu, *Int. J. Hydrogen Energy*, 2012, **37**, 5817–5824.
23. L. G. Xia, Y. H. Guo, Z. Wu and X. B. Yu, *J. Alloys Compd.*, 2009, **479**, 545–548.
24. P. Choudhury, S. S. Srinivasan, V. R. Bhethanabotla, Y. Goswami, K. McGrath and E. K. Stefanakos, *Int. J. Hydrogen Energy*, 2009, **34**, 6325–6334.
25. R. A. Varin and L. Zbroniec, *Int. J. Hydrogen Energy*, 2010, **35**, 3588–3597.
26. R. A. Varin and R. Parviz, *Int. J. Hydrogen Energy*, 2012, **37**, 1584–1593.
27. P. Ngene, M. R. van Zwienen and P. E. de Jongh, *Chem. Commun.*, 2010, **46**, 8201–8203.
28. J. Xu, X. B. Yu, Z. Q. Zou, Z. L. Li, Z. Wu, D. L. Akins and H. Yang, *Chem. Commun.*, 2008, **44**, 5740–5742.
29. V. Tozzini and V. Pellegrini, *J. Phys. Chem. C*, 2011, **115**, 25523–25528.
30. G. Srinivas, Y. Zhu, R. Piner, N. Skipper, M. Ellerby and R. Ruoff, *Carbon*, 2010, **48**, 630–635.
31. J. Xu, R. R. Meng, J. Y. Cao, X. F. Gu, Z. Q. Qi, W. C. Wang and Z. D. Chen, *Int. J. Hydrogen Energy*, 2013, **38**, 2796–2803.
32. Y. Zhu, S. Murali, M. D. Stoller, K. J. Ganesh, W. Cai, P. J. Ferreira, A. Pirkle, R. M. Wallace, K. A. Cychosz, M. Thommes, D. Su, E. A. Stach and R. S. Ruoff, *Science*, 2011, **332**, 1537–1541.
33. B. J. Li, H. Q. Cao, J. F. Yin, Y. A. Wu, J. H. Warner, *J. Mater. Chem.*, 2012, **22**, 1876–1883.
34. L. Ren, K. S. Hui and K. N. Hui, *J. Mater. Chem. A*, 2013, **1**, 5689–5694.
35. Z. Y. Ji, X. P. Shen, G. X. Zhu, H. Zhou and A. H. Yuan, *J. Mater. Chem.*, 2012, **22**, 3471–3477.
36. K. Bhowmik, D. Sengupta, B. Basu and Goutam De, *RSC Adv.*, 2014, **4**, 35442–35448.
37. J. W. Liu, T. Yang, L. Y. Ma, X. W. Chen and J. H. Wang, *Nanotechnology*, 2013, **24**, 505704–505712.
38. M. Gaboardi, A. Bliersbach, G. Bertoni, M. Aramini, G. Vlahopoulou, D. Pontiroli, P. Mauron, G. Magnani, G. Salviati, A. Züttel and M. Riccò, *J. Mater. Chem. A*, 2014, **2**, 1039–1046.
39. B. C. Weng, X. B. Yu, Z. Wu, Z. L. Li, T. S. Huang, N. X. Xu and J. Ni, *J. Alloys Compd.*, 2010, **503**, 345–349.
40. J. Xu, R. R. Meng, J. Y. Cao, X. F. Gu, W. L. Song, Z. Q. Qi, W. C. Wang and Z. D. Chen, *J. Alloys Compd.*, 2013, **564**, 84–90.
41. J. H. Her, M. Yousufuddin, W. Zhou, S. S. Jalisatgi, J. G. Kulleck, J. A. Zan, S. J. Hwang, R. C. Jr. Bowman and T. J. Udovic, *Inorg. Chem.*, 2008, **47**, 9757–9759.

Highly-dispersed Ni/G catalysts were synthesized via a facile hydrogen thermal reduction method and utilized to enhance the de-/rehydrogenation properties of $LiBH_4$.